

Article

Engineering the Tensile Response of Glass Textile Reinforced Concrete for Thin Elements

Sachin Paul * and Ravindra Gettu 

Department of Civil Engineering, Indian Institute of Technology Madras, Chennai 600036, India; gettu@iitm.ac.in
* Correspondence: sachinmmp@gmail.com

Abstract: Textile-reinforced concrete (TRC) is a composite made with bi-directional non-metallic fabric embedded in a fine-grained cementitious matrix. When engineered appropriately, these composites can reduce material usage for the desired performance, resulting in slimmer sections and enhanced material efficiency, which in turn lowers the CO₂ footprint. To facilitate the widespread application of TRC in practice, it is crucial to comprehend the material and structural behavior of these composites, which can pave the way toward an optimized design methodology. In this paper, the tensile response of TRC is studied with different textile geometries, volume fractions and matrix strengths. The influence of the coating impregnation on the effectiveness of the textile to enhance the response of the composite is discussed, with complementing evidence from microstructural observations. The results of tests with different textile configurations indicate a transition in the type of stress–strain response from tri-linear to bi-linear, beyond a certain effective volume fraction. The paper also presents a simplified model to predict the bi-linear response from the efficiency factor-based approach. The insights gained can assist in achieving composite designs with optimized sections and limited tensile stress cracking, ensuring the targeted performance in slender elements.

Keywords: textile-reinforced concrete; tensile response; textile coating; fracture; toughening



Citation: Paul, S.; Gettu, R. Engineering the Tensile Response of Glass Textile Reinforced Concrete for Thin Elements. *Sustainability* **2023**, *15*, 14502. <https://doi.org/10.3390/su151914502>

Academic Editors: Nele De Belie and Anibal C. Maury-Ramirez

Received: 9 August 2023

Revised: 29 September 2023

Accepted: 3 October 2023

Published: 5 October 2023



Copyright: © 2023 by the authors. Licensee MDPI, Basel, Switzerland. This article is an open access article distributed under the terms and conditions of the Creative Commons Attribution (CC BY) license (<https://creativecommons.org/licenses/by/4.0/>).

1. Introduction

The most sustainable options in construction, in terms of reducing the carbon footprint, involve the choice of the right structural system, minimization of the element dimensions (for lower raw material consumption) and increasing the durability (for more efficient exploitation of resources). Textile-reinforced concrete (TRC) presents a unique advantage in this regard, enabling the construction of lightweight, durable and modular structural elements, while eliminating the risk of curtailed service life due to corrosion [1]. Comprising bi-directional non-metallic fabric embedded in a fine-grained cementitious matrix, TRC exhibits high tensile strength, proving to be a viable solution for both the construction of slender elements and the retrofitting of existing structures [1–3]. This innovative combination of the concepts of mesh reinforcement with fiber-reinforced concrete effectively addresses the limitations of durability and crack width control in both of those systems [4].

TRC provides an environmentally sustainable option by substantially reducing concrete usage [4,5], thereby reducing the impacts associated with conventional reinforced concrete, including a reduction in the use of materials like portland cement and steel. The non-corrosive reinforcement (i.e., glass or carbon) in TRC contributes to its durability, which enhances sustainability. Overall, such aspects lead to a significant decrease in embodied emissions and energy, raw material consumption and waste generation [6].

Most applications of TRC have been in thin-walled tensile and flexural members. However, with a better understanding of its response, the rational design of more complex TRC elements is becoming a reality. Substantial work in this area has been reported in many state-of-the-art reports [1–4], and the results are encouraging with respect to the performance of these composites in terms of limiting crack propagation during failure and

enhancing tensile strength and strain capacity. The response of TRC is, however, influenced by several factors, such as the material characteristics and geometric parameters of the reinforcement, and its volume fraction. High-moduli, high-strength fabrics, such as those of carbon, glass and aramid, impart high strength and toughness to the composite [7,8], and are consequently more desirable as reinforcement.

The tensile stress–strain response of TRC composites is conventionally represented by three distinct zones [9,10]. The initial phase—Zone I—pertaining to the linear response, is governed by the stiffness of the matrix, until first cracking. Due to the relatively low fiber volume fractions, the contribution of the textile to the overall stiffness of the composite is negligible in this zone. After the first crack, a further increase in load leads to the development of multiple cracks, which manifests as a nonlinear zone of the tensile response (Zone II). A significant drop in stiffness is observed in this zone, with its extent and number of cracks being dependent on the amount of reinforcement, the textile geometry, and the bond between the textile and matrix [11–15]. Often, cracking is observed to occur at almost constant or decreasing stress. The next phase (i.e., Zone III) of the stress–strain response is of the strain-hardening type, with a practically linear response, governed by the properties of the reinforcement. In this stage, all the load is carried by the textile yarns, and the existing cracks widen until the fabric, bridging one of the cracks, ruptures. The final failure could also be accompanied by the pullout of the yarns, depending on the geometry of the composite element [16,17]. In some cases, the response is practically bi-linear, with the absence of a distinct Zone II, yielding higher load-carrying capacity at the same strain, when compared with a composite with a tri-linear response.

The nature of the individual fibers that make up each yarn, the coating material [18–20] and the level of impregnation [21] are crucial for the micro-mechanics of the composite, especially in terms of the stress distribution at the matrix–fabric interface. The interaction between the inner and outer fibers of yarns determines if their response in the composite is monolithic or telescopic [21,22]. A fully impregnated fabric behaves more monolithically, with uniform stress distribution across the yarn, whereas partial impregnation results in higher stresses in the exterior fibers causing a reduction in the ultimate tensile capacity of the composite due to telescopic failure. Stiffer coating materials, such as epoxy, are observed to impart better uniformity of the stress distribution in the yarn, and therefore, yield higher tensile strength, in comparison to softer styrene–butadiene rubber (SBR) or acrylic-based coated systems [19,23,24]. Furthermore, the durability and aging of fibers within the cementitious system can also alter the final behavior of the composite [25–27].

The matrix composition and the specimen geometry can significantly influence the response of TRC composites [11,16,28]. Using a matrix with lower strength can reduce the bond between the textile and the matrix, resulting in potential failure due to fiber pullout or slippage [23,29,30]. The incorporation of short fibers can improve the bond, especially when utilizing low-strength mixtures [31,32].

It should also be noted that the experimental procedure used for characterizing the tensile response of the composite can influence the type of failure. Earlier research predominantly endorsed rotating end conditions during uniaxial tensile testing of TRC [11,33,34]. However, more recent studies apply partially clamped boundary conditions, where the grips mitigate textile slippage, curbing pullout failure [14,21,35]. However, reports indicate that the end conditions are especially important for uncoated textiles, compared to those that are partially or fully impregnated [36,37], or for specimens that are warped or have misaligned reinforcement [38].

Several approaches for the prediction of the overall response of TRC can be seen in the literature. Two early analytical models were the ACK model [39] and the Cuypers model [40], both of which are based on the tri-linear model for the stress–strain behavior, with the initial response based on the method of mixtures and the final strain-hardening zone based only on the textile response. The difference between the two models lies in the second phase, where the ACK model considers multiple cracking at constant stress levels while the Cuypers model contemplates crack formation at progressively increasing stress

based on the Weibull distribution. However, several studies indicate that these models may not always represent the true behavior of TRC [41,42]. A more recent analytical approach is based on the global stiffness governed by cracking behavior and stress drops at each crack [43]. Another model accounts for the bond-lag behavior between the core and sleeve filaments to obtain the composite response [21]. Even though both these approaches can predict the TRC behavior with reasonable accuracy, the input parameters for the modeling require complex experimental procedures. The present study attempts to complement the more sophisticated models by developing a simplified methodology for representing the tensile response of TRC based on efficiency factors.

An important aspect of the design of TRC for sustainability is the decision on the number of layers of reinforcement or volume fraction for a given matrix, to provide the desired load-carrying capacity for an allowable strain with the least element thickness. Despite earlier research, there is a deficit in the understanding of the tensile behavior of TRC when considering varying textile configurations and reinforcement ratios, which is critical for an optimized design approach for achieving better sustainability. Accordingly, an objective of this paper is to propose a criterion for choosing the minimum number of layers that result in the highest load-carrying capacity at a given strain. This concept is illustrated here with several types of textiles embedded in two different cementitious matrices, by analyzing the composite tensile behavior.

2. Materials Used

2.1. Textiles

Six types of bi-directional woven glass fiber textiles were used in the study (see Table 1 for the geometry and characteristics). The architecture and weaving patterns of the different textiles (denoted F1 to F6) are shown in Figure 1. Textile F2 is an alkali-resistant (AR) glass textile, with zirconium, and the others are E-glass textiles with alkali-resistant coatings. Fourier transform infrared spectroscopy (FTIR) analysis indicates that the coatings on the F1, F3, F4, F5, and F6 textiles contain styrene–butadiene, and that F2 is coated with an acrylic-based product. The textiles have different mesh opening sizes, yarn densities, and tensile strength. In the current study, testing and analysis focus solely on the weft direction (the widthwise orientation that is strongest for the selected fabrics). The cross-sectional area of the textile yarn was calculated from the TEX value provided by the manufacturer and verified by weighing the fibers after removing the coating by thermal treatment. The tensile strength of the single yarn, in each case, was determined as per ASTM D6637/D6637M-15 (Test Method A) [44].

Table 1. Properties of the textiles used.

Textile	Coating Material ^a	Opening Size ^c [mm × mm]	Mass per Unit Textile Area with the Coating ^c [g/m ²]	Nominal Cross-Section Area of a Single Weft Yarn ^b [mm ²]	Measured Weft Yarn Tensile Strength [MPa]
F1	SBR	8.5 × 6.5	267	0.79	1168 ± 103
F2	Acrylic	25.0 × 25.0	180	0.92	1040 ± 102
F3	SBR	15.7 × 10.1	280	0.92	1144 ± 133
F4	SBR	8.0 × 8.0	178	0.31	1367 ± 86
F5	SBR	9.0 × 10.0	118	0.31	1393 ± 76
F6	SBR	4.0 × 4.5	117	0.13	1483 ± 12

^a From FTIR analysis; SBR: styrene–butadiene rubber. ^b Calculated based on the TEX value provided by the manufacturer. ^c Details provided by the manufacturers.

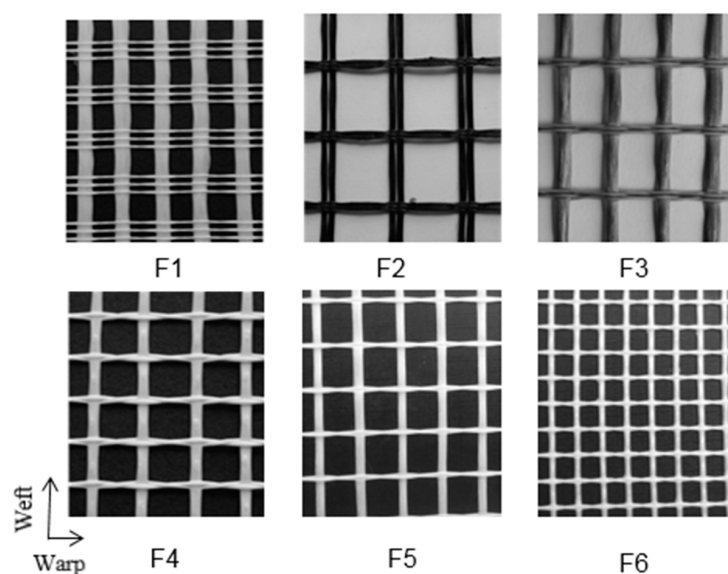


Figure 1. Types of textiles used in the study.

2.2. Cementitious Matrices

The matrix used for TRC is required to possess high flowability for adequate penetration between layers of textile in thin elements. In view of this, two self-consolidating matrices were developed with a relatively high binder content. A polycarboxylate-based superplasticizer was used to obtain the desired rheology. The matrix M1 had a water–binder ratio of 0.4 and a moderate compressive strength of 60.2 ± 2.7 MPa while the higher-strength mix M2 had a water–binder ratio of 0.24 and a compressive strength of 104.1 ± 4.2 MPa. The binder for both mixes was a blend of ordinary portland cement, ASTM Class F fly ash and silica fume. A hydroxypropyl methylcellulose-based viscosity modifying agent (VMA) was used in mix M2 for better stability. The maximum size of aggregates was limited to about 1 mm to facilitate uniform penetration of the matrix between the textile layers. The mix proportions and the mechanical properties of the mixes are given in Table 2. The compression tests were conducted in accordance with IS 4031 on 70.6 mm cube specimens. The flexural test was carried out as per ASTM C348 standards, with specimens of $40 \times 40 \times 160$ mm dimensions. The matrix tensile strength was derived from the uniaxial test following the RILEM TC 232-TDT (2016) guidelines [33]. All samples were tested after 28 days of curing in a mist room, at a temperature of 25 ± 2 °C.

Table 2. Mix proportions and mechanical properties (mean \pm standard deviation) of the fine-grained concrete.

Materials/Properties	Mix M1	Mix M2
Cement (kg/m ³)	583	674
Fly ash (kg/m ³)	208	114
Silica fume (kg/m ³)	42	79
Quartz sand, 0.2–1.1 mm (kg/m ³)	595	1037
Quartz powder, 20–160 μ m (kg/m ³)	357	207
Water/binder	0.40	0.24
PCE superplasticizer (% solids/binder by weight)	0.15	1.30
VMA (% solids/binder by weight of binder)	-	0.08
28-day cube compressive strength (MPa)	60.2 ± 2.7	104.1 ± 4.2
28-day flexural strength (MPa)	7.2 ± 0.1	11.8 ± 0.2
28-day tensile strength (MPa)	3.9 ± 0.2	5.8 ± 0.3
Modulus of elasticity (GPa)	27.1 ± 1.8	34.6 ± 1.7

3. Experimental Programme

3.1. Specimen Preparation

All the specimens, of 500 mm length and 60 mm width, were molded as per the geometry specified by RILEM TC 232-TDT (2016); see Figure 2. The thickness was kept at 10.0 mm, except for the five-layer configurations of F2 and F3 textiles for which it was increased to 11.2 mm. The specimens were cast in steel molds with screw-down end plates. The textiles were positioned horizontally in layers with steel spacers at the edges, and the matrix mix was poured into the mold. Five specimens were cast for each configuration and maintained at room temperature (about 25 °C) for 24 h, after which they were demolded, and cured in a mist room at 25 ± 2 °C for 28 days. The nomenclature of the specimens presented in the study is T-FM-nL: where T indicates the tensile test, F—the textile type (i.e., F1 to F6), M—matrix used (i.e., M1 or M2) and nL—number of layers (i.e., 1 to 5).

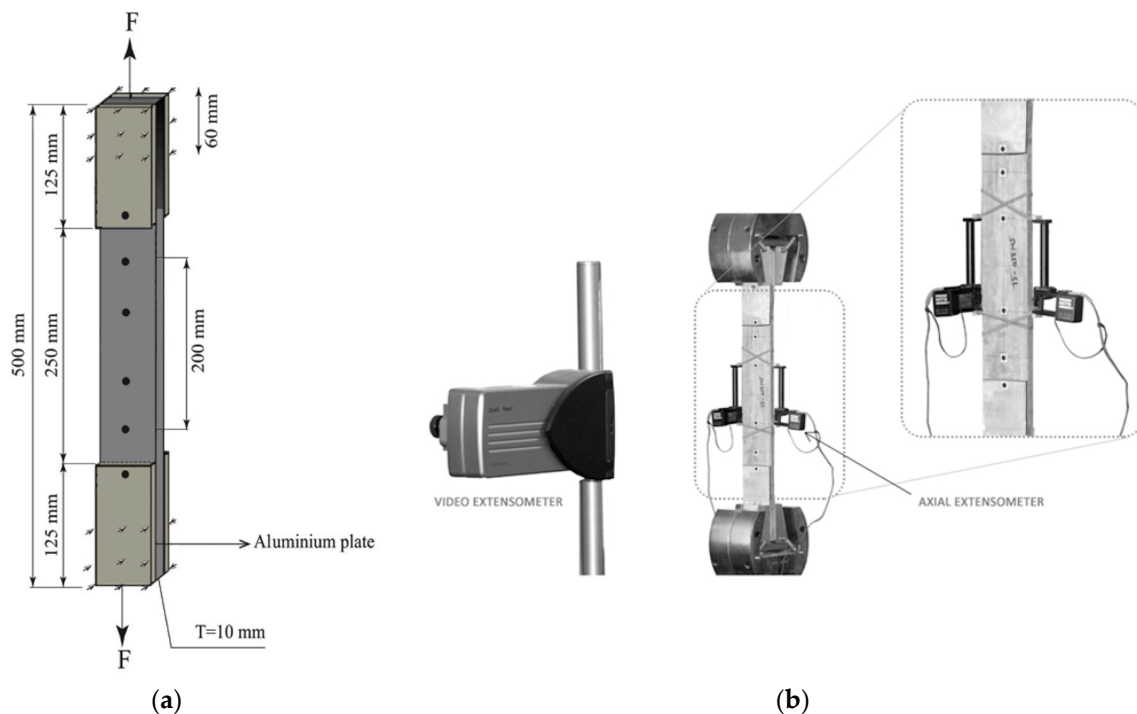


Figure 2. (a) Geometry of the specimen and (b) uniaxial tensile test setup.

3.2. Experimental Setup

The uniaxial tensile tests (Figure 2) were carried out in a servo-controlled electromechanical system with a 50 kN load cell, as shown in Figure 2b. Aluminum end plates of 2 mm thickness with rectangular geometry were glued to the gripping zone to avoid local crushing at the supports during testing, and screw grips were used to mount the specimens on the machine. The tests were performed at a constant displacement rate of 0.8 mm/min. A combination of signals from video and strain gauge-based axial extensometers was used to obtain the displacement of the specimen. The axial extensometer was used to measure the strain in the composite until the first crack, and the video extensometer, measuring the relative displacement over a 200 mm gauge length, was used for the remaining portion of the curve. This method was adopted to mitigate the influence of the noise in the video extensometer signal at the low displacement range. It is to be noted that though some cracking occurred outside the gauge length, the strains calculated were consistent. Specimens exhibiting failure in the end zone or clamping area were discarded from the analysis.

4. Results and Discussions

In all the cases, the stress values were obtained by dividing the measured load by the gross cross-sectional area of the composite. The stress corresponding to the first crack was

identified from the first drop in the initial linear portion of the stress–strain response, after which there was a sudden change in the slope.

4.1. Effect of Textile Geometry on Stress-Response and Crack Formation

The textiles F1 and F2 are both leno woven but have different geometries and reinforcement ratios (see Table 1). The typical stress–strain responses of the composites with one to four layers of textile F1 and one to five layers with textile F2 in the matrix M1 are shown in Figure 3, and the average stress and strain values are reported in Table 3. In these cases, the specimens exhibited distributed cracking, with the number of cracks increasing with the reinforcement ratio and the crack widths consequently reducing. For lower reinforcement ratios, such as in F1M1-1L and -2L, and F2M1-1L and -2L, the ultimate rupture occurred near the mid-length of the specimen. However, for higher reinforcement ratios, the failure occurred in the vicinity of the endplates. Visual examination revealed that the first crack occurs near the fill yarns, possibly due to weakening of the cross-section at these locations, especially for high fill yarn volume fraction or fill yarns with larger cross-sections. However, at higher reinforcement ratios, additional cracks form between the fill yarns.

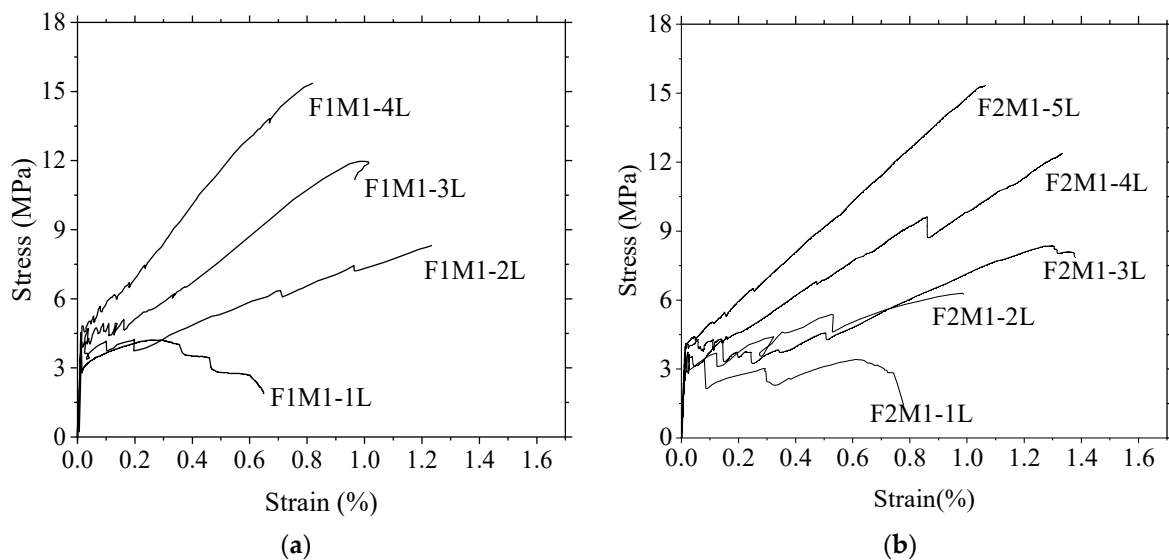


Figure 3. Typical stress–strain responses of M1 matrix reinforced with different layers of (a) F1 and (b) F2 textiles.

As observed from Figure 3, specimens F1M1-1L and F2M1-1L with single layers of reinforcement showed strain-softening behavior, without multiple cracking. With an increase in reinforcement ratio, the composite response changes to the strain-hardening type with multiple cracking. The tensile response of specimens F1M1-2L and F2M1-2L with two layers of textile did not have any distinct crack stabilization phase whereas specimens F1M1-3L, F2M1-3L and F2M1-4L exhibit typical tri-linear behavior with multiple cracking under almost constant stress, followed by the widening of the cracks under increasing stress. However, a few new cracks were observed to form in some of the specimens during the strain-hardening regime. Further increase in reinforcement (i.e., in specimens F1M1-4L and F2M1-5L) leads to a transition in the nature of the stress–strain response from tri-linear to bi-linear, with multiple cracking occurring as the stress increases. It is evident that composites with bi-linear response exhibit much better load-carrying capacities at the same strains when compared to those with tri-linear behavior.

Considering the stress and strain values given in Table 3, it is seen that the ultimate strains are higher for lower reinforcement ratios and that an increase in the reinforcement ratio leads to higher stiffness in the strain hardening regime, as expected, with a reduction in the ultimate strain of the composite.

Table 3. Parameters of tensile response of the composites.

Specimen	First Peak		Intermediate Stress at Different Strains				Ultimate Peak		Number of Cracks
	Stress	Strain	0.2%	0.4%	0.8%	1.2%	Stress	Strain	
F1M1-1L	3.38 ± 0.51	0.013 ± 0.0014	3.73 ± 0.21	3.47 ± 0.73	1.75 ± 0.78	-	4.08 ± 0.23	0.31 ± 0.11	1
F1M1-2L	3.4 ± 0.65	0.0126 ± 0.0015	3.66 ± 0.37	3.89 ± 0.47	5.49 ± 0.41	6.46 ± 0.44	6.84 ± 0.36	1.33 ± 0.15	7
F1M1-3L	4.03 ± 0.75	0.0164 ± 0.0052	5.092 ± 0.60	6.704 ± 0.45	10.12 ± 0.44	-	11.37 ± 0.44	1.10 ± 0.041	10
F1M1-4L	5.15 ± 0.41	0.0198 ± 0.0026	7.84 ± 0.24	10.51 ± 0.77	15.31 ± 0.25	-	15.80 ± 0.36	0.91 ± 0.054	15
F2M1-1L	3.11 ± 0.62	0.0114 ± 0.0025	2.8 ± 0.30	2.5 ± 0.76	1.37 ± 1.30	-	3.14 ± 0.30	0.63 ± 0.23	1
F2M1-2L	3.86 ± 0.426	0.0142 ± 0.003	3.67 ± 0.34	4.42 ± 0.4	4.88 ± 1.00	3.98 ± 1.6	5.62 ± 0.9	0.99 ± 0.22	7
F2M1-3L	3.51 ± 0.26	0.0126 ± 0.0005	4.17 ± 0.66	4.47 ± 0.53	6.02 ± 0.13	7.96 ± 0.15	8.45 ± 0.10	1.40 ± 0.10	7
F2M1-4L	4.05 ± 0.20	0.0142 ± 0.0014	4.53 ± 0.28	5.78 ± 0.55	9.04 ± 1.02	11.99 ± 0.90	12.26 ± 0.91	1.26 ± 0.04	10
F2M1-5L	4.39 ± 0.28	0.0165 ± 0.002	6.24 ± 0.5	9.56 ± 0.86	14.67 ± 0.47	-	15.13 ± 0.54	1.09 ± 0.03	15
F3M1-4L	3.83 ± 0.37	0.013 ± 0.002	4.02 ± 0.43	6.03 ± 0.36	10.53 ± 0.42	12.21 ± 0.86	12.58 ± 1.03	1.23 ± 0.13	13
F3M1-5L	4.32 ± 0.52	0.016 ± 0.006	6.83 ± 0.38	9.43 ± 0.92	15.32 ± 1.12	-	16.63 ± 0.86	1.06 ± 0.09	17
F4M1-4L	3.32 ± 0.61	0.0118 ± 0.0025	3.52 ± 0.36	3.88 ± 0.73	5.43 ± 1.30	-	7.35 ± 0.35	1.13 ± 0.048	9
F4M1-5L	3.46 ± 0.43	0.0124 ± 0.0018	3.72 ± 0.24	4.13 ± 0.23	6.96 ± 0.83	-	9.34 ± 0.56	1.15 ± 0.032	13
F1M2-3L	5.62 ± 0.45	0.016 ± 0.0012	5.96 ± 0.52	7.68 ± 1.01	10.54 ± 1.31	-	11.13 ± 0.76	0.816 ± 0.016	10
F1M2-4L	5.67 ± 0.38	0.0168 ± 0.0026	7.67 ± 0.24	10.56 ± 0.77	-	-	15.32 ± 0.36	0.789 ± 0.034	14
F2M2-4L	5.23 ± 0.23	0.0152 ± 0.0018	5.82 ± 0.27	6.96 ± 0.32	11.56 ± 52	-	11.63 ± 0.36	0.802 ± 0.05	15
F2M2-5L	5.63 ± 0.34	0.0171 ± 0.002	8.93 ± 0.42	11.32 ± 0.86	-	-	15.03 ± 0.54	0.74 ± 0.02	15
F3M1-4L	5.33 ± 0.42	0.016 ± 0.003	5.86 ± 0.46	7.56 ± 0.58	-	-	11.03 ± 1.03	0.89 ± 0.16	11
F3M2-5L	5.16 ± 0.18	0.015 ± 0.003	7.96 ± 0.36	10.86 ± 0.75	15.83 ± 1.36	-	16.13 ± 1.43	0.88 ± 0.12	16

The effect of concrete strength on the stress–strain response of the composites can be studied by comparing the responses of specimens with the F1 and F2 textiles in the M1 (60 MPa) and M2 (104 MPa) matrices. It is seen from the typical curves shown in Figure 4 and the data in Table 3 that the first-crack strength of the composite was 30–55% higher for the M2 mix in comparison to the M1 mix and the ultimate strain was lower, as expected. However, the number of cracks was observed to be in the same range for both matrices, which indicates that the textile characteristics govern the spacing of the cracks. Evidently, the composites with the M2 matrix also exhibit a transition in the response from softening to tri-linear to bi-linear.

In general, the first-crack stress is observed to be marginally less for a TRC composite with a low reinforcement ratio than that of plain mortar. This could be attributed to the reduction of the cross-section near the fill yarns. However, with an increase in the reinforcement ratio, the first-crack stress is found to be in the same range or higher for the composite in comparison to that of the mortar. Further, it is seen that the first-crack stress increases with reinforcement ratio in closely spaced textile configurations. For example, F1M1-4L exhibits 51% higher first-crack stress than the composite with the two-layer configuration of the same textile (F1M1-2L). However, the first-crack response seems to be strongly influenced by the textile geometry, as observed in the cases of textiles F2 and F3 with yarn spacing 25 mm and 16.5 mm, respectively, where there is no significant enhancement in the first-crack stress even with 5 layers of textiles.

To further explore the influence of the textile geometry on the first-crack stress, tests were performed with two textiles F5 and F6 having a similar reinforcement ratio but different yarn spacing. Textile F5 had a relatively larger opening size of 9.0 × 10.0 mm and F6 had an opening size of 4.0 × 4.05 mm. The typical stress–strain responses of F5TM1-4L and F6TM1-4L are shown in Figure 5; it is observed that the first-crack load with 4 layers of F6 textiles was 40% higher than that observed with 4 layers of F5 textiles. The reason for the higher first-crack stress with the textiles of closer yarn spacing can be attributed to more effective arresting of the microcracks, thereby avoiding interconnected cracking and a drop in the strength of the composite.

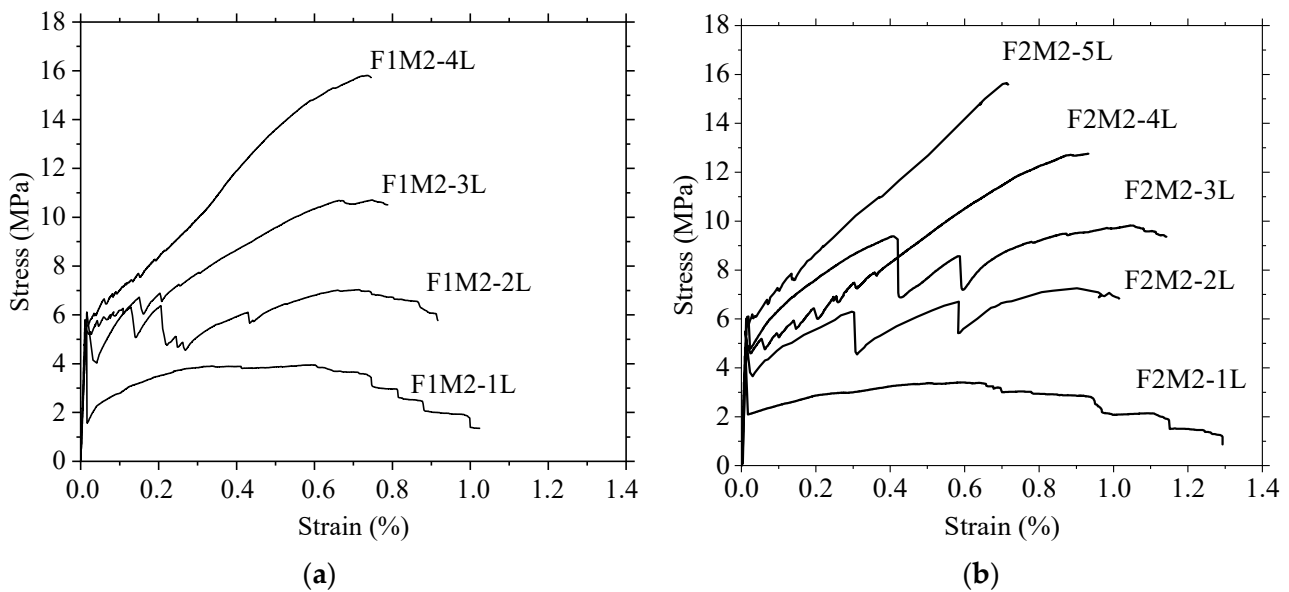


Figure 4. Typical stress–strain responses of specimens with M2 (104 MPa) matrix and different layers of (a) F1 and (b) F2 textiles.

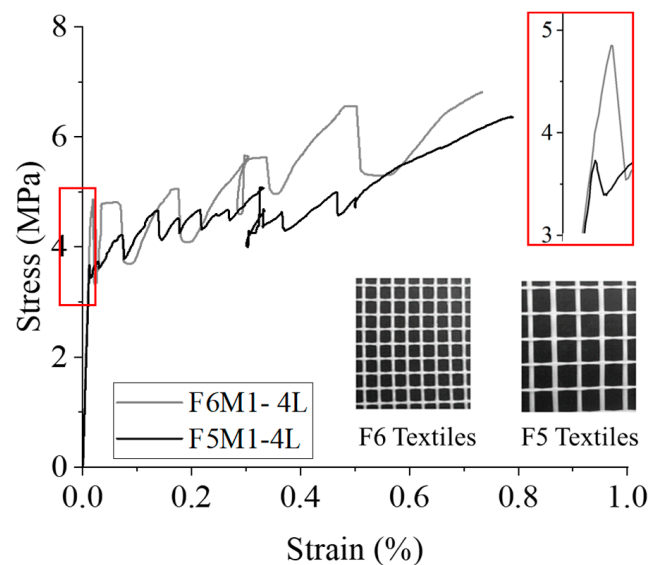


Figure 5. Typical stress–strain response of composite with 4 layers of F5 and F6 textiles.

4.2. Efficiency Factor

The relation between the nominal stress in the textile in the composite at failure and the tensile strength of the yarn is often expressed as the efficiency of the textile in terms of a factor, which can be defined as

$$k = F_{ct} / (V_t \times f_{tt}) \quad (1)$$

where V_t is the volume fraction of the textile in the direction of tensile loading, and F_{ct} is the tensile capacity of the composite and f_{tt} is the tensile strength of the textile used. The efficiency factor depends on the uniformity of the stress distribution between the outer (sleeve) and the inner (core) fibers of a yarn (Figure 6). Since the outer fibers are bonded to the cementitious matrix and the inner fibers are free to slip, the crack bridging generates tensile stresses mostly in the sleeve fibers, and when these rupture, the inner fibers are progressively stressed until the ultimate collapse of the composite. Therefore, the efficiency

of reinforcement by the textile yarns in the composite is largely dependent on the relative amounts of sleeve and core fibers in the yarn.

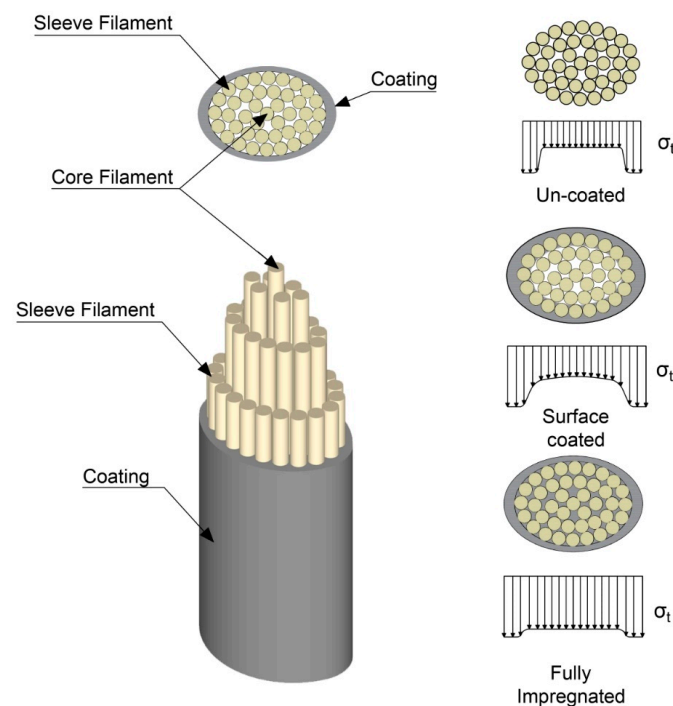


Figure 6. Graphical representation of the core and sleeve fibers in concrete matrix.

The efficiency factors obtained for the different configurations (of textile and matrix) tested here are shown in Figure 7, in terms of average values. It is evident that the values fall in two ranges indicated by the dashed lines. For the SBR-coated textiles, the efficiency factor has an average value of 0.45 ± 0.038 , and for the acrylic-coated textiles, it is observed to be 0.62 ± 0.020 . This implies that only about 45% and 62% of the strength, respectively, are effectively reached in these textiles when the composite ruptures.

An important reason for the difference in the efficiencies of the two types of textile coatings appears to be the uniformity of the coating material on the yarn. The scanning electron microscope (SEM) images in Figure 8 show the cross-section of the yarns of the F1 (Figure 8a), F2 (in Figure 8b), F3 (in Figure 8c) and F4 (in Figure 8d) textile. It should be noted that F2, F3 and F4 have SBR coating, and F2 has an acrylic-based coating. A closer examination of the cross-section of F1 (Figure 8a) reveals loosely held interior fibers surrounded by sleeve fibers, suggesting the occurrence of slip between the core and sleeve, and within the core itself. This is reflected by the lower efficiency factors, with F1 having the lowest average efficiency factor of 0.42. Textile F2 (Figure 1) has two yarns per roving in the weft direction, and the SEM image of one of the yarns, in Figure 8b, shows an evenly distributed coating with good penetration of the acrylic-based material through the yarn cross-section. Consequently, there is proper adhesion between the interior and exterior fibers and an average efficiency factor of 0.62. Textile F3 (Figure 8c) is seen to have a thicker surface coating with low penetration of coating material into the interior in comparison with F2, though better than F1. The larger cross-section of the textile yarn, the elongated shape and the thick coating result in a hollow central core, with the average efficiency factor for F3 textiles being only 0.47. The efficiency factor for F4 (Figure 8d) textiles is marginally higher than the F3 textiles, which can be attributed to the thinner rovings. Similarly, the efficiency factor for F1 textiles with larger cross-sections is 0.42 whereas composites with the textile F6 with the smallest cross-sectional area have an efficiency factor of 0.47. This is due to the reduction of the sleeve-to-core ratio with an increase in the cross-sectional

area. Therefore, it can be generalized that the efficiency factor is influenced by the coating material, the uniformity of the coating and the cross-sectional area of the yarn.

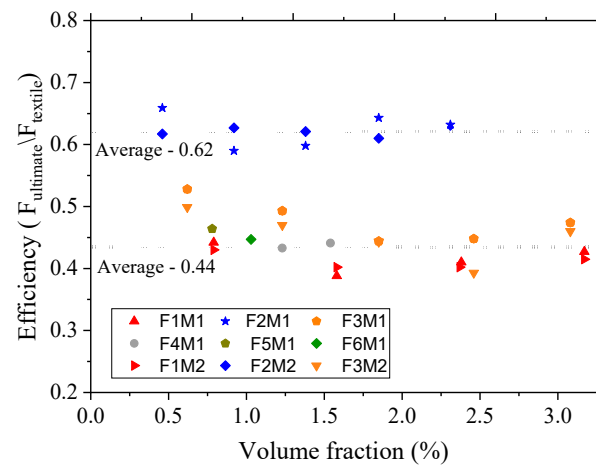


Figure 7. Efficiency factor for the different configurations.

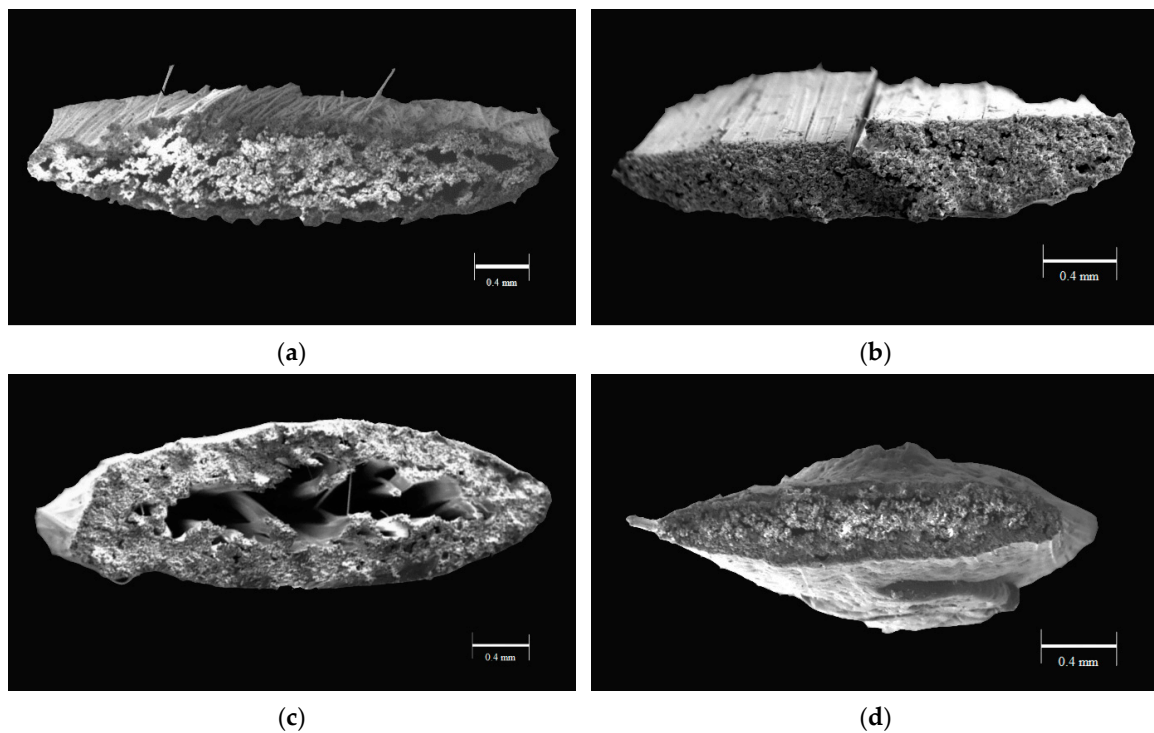


Figure 8. SEM images of the cross-sections of (a) F1, (b) F2, (c) F3 and (d) F4 yarns.

5. Transition in Tensile Response from Tri-Linear to Bi-Linear

As seen earlier, the tensile behavior of textile-reinforced concrete can be idealized as being tri-linear or bi-linear, except when low reinforcement causes strain softening. As seen in the tests performed here, the response of the composite is characteristically bi-linear, beyond a certain reinforcement ratio, with multiple cracking occurring as the stress level progressively increases after the first crack, resulting in a strain-hardening type response, without any plateau. For such specimens, crack stabilization (or the absence of new cracks) occurs at a higher strain level than those with a tri-linear response. With a higher strength matrix, the bi-linear response occurs with fewer layers, suggesting that the better bond between the textile and yarn enhances the toughening in the composite. On the other

hand, textiles with lower cross-section areas need more layers for the transition to occur (e.g., F4M1-5L versus F1M1-4L).

For any given matrix, the transition in the stress–strain behavior can be related to an effective volume fraction, defined as the product of the efficiency factor and volume fraction (see Table 4), which indicates the proportion of fibers that contribute to the tensile resistance of the composite. It is observed, in the present study, that the transformation from tri-linear to bi-linear occurs when the effective volume fraction crosses a threshold of about 1.3, except for F2M2-4L, which can be attributed to the higher bond strength and better performance of the acrylic coating.

Table 4. Effective volume fraction.

Composite	Volume Fraction (V_t)	Average Efficiency Factor (k)	Average Effective Volume Fraction	Behavior
F1M1-3L	2.38	0.43	1.02	tri-linear
F1M1-4L	3.17	0.41	1.30	bi-linear
F2M1-4L	1.85	0.64	1.18	tri-linear
F2M1-5L	2.31	0.63	1.46	bi-linear
F3M1-4L	2.46	0.45	1.11	tri-linear
F3M1-5L	3.08	0.47	1.45	bi-linear
F4M1-4L	1.23	0.42	0.52	tri-linear
F4M1-5L	1.54	0.43	0.66	tri-linear
F1M2-3L	2.38	0.42	1.00	tri-linear
F1M2-4L	3.17	0.41	1.30	bi-linear
F2M2-4L	1.85	0.63	1.17	bi-linear
F2M2-5L	2.31	0.61	1.41	bi-linear
F3M1-4L	2.46	0.46	1.13	tri-linear
F3M2-5L	3.08	0.44	1.36	bi-linear

The transition of the tensile response from tri-linear to bi-linear can be explained based on the phenomena involved in the cracking and its propagation. As the tensile stress increases, cracking is initiated at some regions that could be statistically weaker than other regions with similar tensile stresses. The crack propagates (with a drop in load-carrying capacity) until it is arrested from progressing further by the textile yarn(s) that bridge(s) the crack tip. For the crack to propagate beyond the yarn(s), a much higher stress would be required. Consequently, cracks initiate at other sections of the composite member as the local tensile strengths at these points are reached. This leads to multiple cracking in TRC with little or no significant increase in load-carrying capacity. Later, mobilization of energy dissipation mechanisms, such as crack bridging and pullout, increases the crack resistance and the load-carrying capacity, resulting in the tri-linear response. However, when the reinforcement level is higher (or denser), the toughening is more effective, and as each crack initiates and is arrested, the stress progressively increases, resulting in a strain-hardening type or bi-linear response.

Considering the bi-linear behavior to be desirable in the composite due to the phenomena discussed earlier, it can be idealized as consisting of two phases for the purposes of structural design [45,46]. The first phase, until the first crack, can be characterized using the law of mixtures based on the moduli of elasticity of the textile yarns (E_t) and matrix (E_m), with the modulus of the elasticity of the composite represented by:

$$E_c = E_t V_t + E_m (1 - V_t) \quad (2)$$

where V_t is the volume fraction of the textile in the direction of loading. Since V_t is generally small, the initial response is dominated by the properties of the matrix. The first-crack stress can be considered for practical purposes to be the tensile strength of the plain matrix (f_{mt}).

The second (strain-hardening) part of the composite response is taken to be the product of the elastic modulus of the textile, the efficiency factor and the volume fraction of the fabric:

$$E_h = k V_t E_t. \quad (3)$$

The ultimate tensile stress of the composite or its tensile strength (F_{ct}) can be obtained from the efficiency factor, the volume fraction of the textile and the strength of the textile (f_{tt}), as follows:

$$F_{ct} = k V_t f_{tt}. \quad (4)$$

Several bi-linear responses modeled with the above equations are compared with the corresponding experimental results in Figure 9.

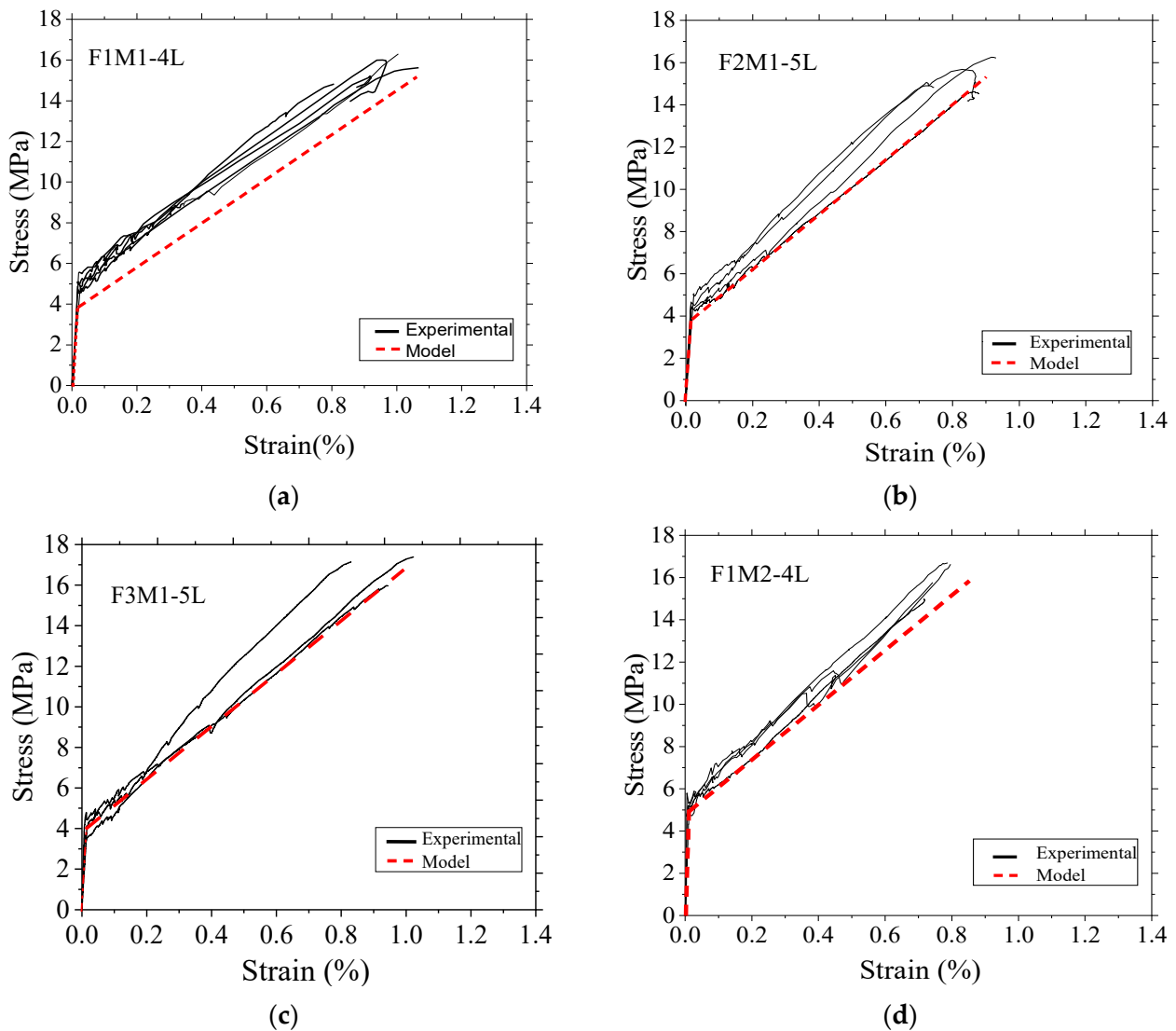


Figure 9. Cont.

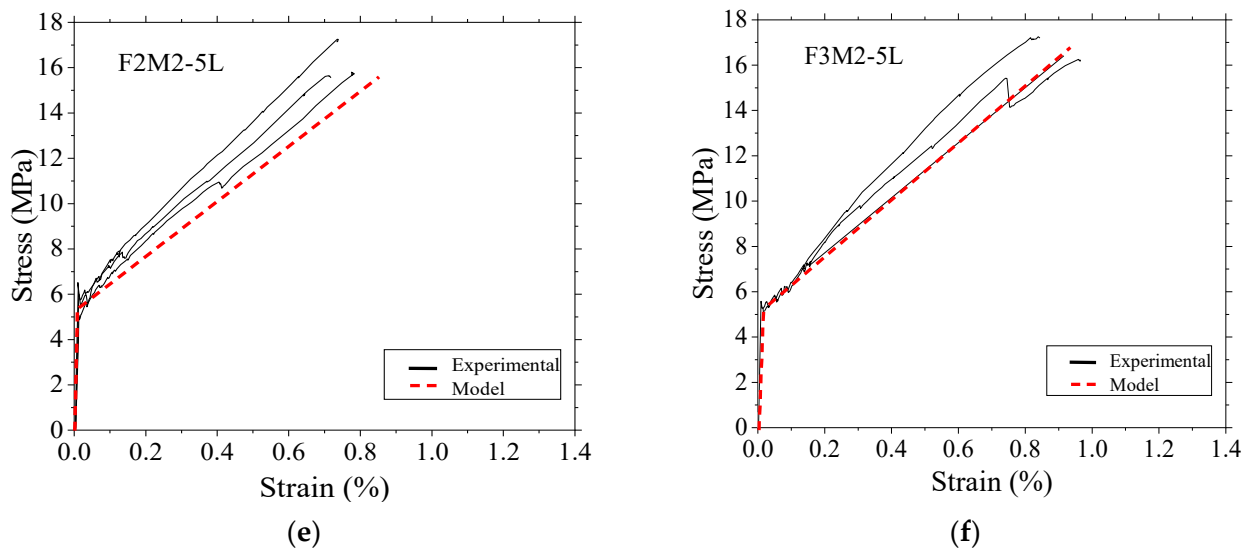


Figure 9. Comparison of the stress–strain response from the model with experimental data for composites with matrices M1 (a–c) and M2 (d–f).

From the results, it can be observed that the proposed model can represent the overall tensile behavior of the composite within acceptable limits. It should be noted that the model is conservative in cases where the first-crack strength is enhanced due to the closer grid spacing of yarns at a high reinforcement ratio (as in Figure 9a). More importantly, the model can be used to design the composite system even though test data are not available for the volume fractions or number of layers that are required. This could lead to more efficient material utilization with the appropriate composite thickness and textile layers.

6. Summary and Conclusions

This paper investigates the tensile response of textile-reinforced concrete (TRC) with six types of glass fabrics in two different fine-grained concrete matrices. Composites with multiple layers of textiles were tested to evaluate the influence of the reinforcement ratio on the tensile response. Based on the experimental results, an efficiency factor is obtained for determining the maximum contribution of a given type of textile in a certain matrix. Further, it is seen that a simple model based on this factor can represent the bi-linear response of TRC under tension. Using the model and the understanding gained, the potential to engineer thin elements that are not only optimized for higher performance but also embody principles of sustainability by reducing raw material consumption and cement usage.

Some specific findings from the study are summarized below:

- The first crack in the composite develops mostly in the vicinity of the cross-yarn, especially at lower reinforcement ratios. However, at higher reinforcement ratios, cracks were observed to develop between the cross yarns.
- Though the first-crack strength depends mainly on the matrix properties, it was observed that it could be enhanced by the geometry of the fabric. A closer yarn configuration at a higher reinforcement volume was seen to result in higher first-crack stress than the matrix tensile strength.
- For the textiles used in the study, the tensile response of the composite changes from strain-softening to strain-hardening as the number of layers increases, with a transition from a tri-linear to a bi-linear response.
- The effectiveness of the textiles in the composite is influenced significantly by the type and extent of the penetration of the coating material into the yarns.
- An efficiency factor has been defined as the ratio between the nominal tensile stress in the textile at the failure of the composite and its tensile strength. This seems to be

independent of the matrix strength or the volume fraction of the particular textile used in the TRC composite.

- From the present study, an effective volume fraction or cross-sectional area of textiles was identified based on the efficiency factor for predicting the threshold for the tri-linear to bi-linear transition.
- A simple model for the bi-linear response of TRC was developed for possible use in design methods, based on the efficiency factor, the volume fraction of the textile used, tensile strength and modulus of elasticity of the matrix, and the modulus of elasticity and strength of the textile. The prediction model compares satisfactorily with the experimental results. This approach would aid in the design for appropriate functionality of these elements with low material usage, leading to better sustainability.

Author Contributions: Conceptualization, S.P. and R.G.; methodology, S.P. and R.G.; formal analysis, S.P.; investigation, S.P.; resources, R.G.; data curation, S.P.; writing—original draft, S.P.; writing—review and editing, R.G.; visualization, S.P. and R.G.; supervision, R.G.; project administration, R.G.; funding acquisition, R.G. All authors have read and agreed to the published version of the manuscript.

Funding: Partial funding for this study was provided by the CRG/2019/004267 grant from the Science and Engineering Research Board (SERB), Government of India.

Institutional Review Board Statement: Not applicable.

Informed Consent Statement: Not applicable.

Data Availability Statement: Not applicable.

Acknowledgments: The first author is thankful to the Ministry of Education, Government of India, for providing an assistantship during his doctoral studies, under the QIP scheme. Partial funding for this study was provided by the CRG/2019/004267 grant from the Science and Engineering Research Board (SERB), Government of India. The FIST Grant SR/FST/ETII-054/2012 is gratefully acknowledged for the equipment in the Laboratory for Mechanical Performance of Civil Engineering Materials, IIT Madras. This work was carried out in the Centre of Excellence on Technologies for Low-carbon and Lean Construction at IIT Madras.

Conflicts of Interest: The authors declare no conflict of interest.

References

1. Brameshuber, W. (Ed.) *Textile Reinforced Concrete: State-of-the-Art Report of RILEM Technical Committee 201-TRC*; RILEM Publications: Bagnaux, France, 2006; Volume 36.
2. Mobasher, B. *Mechanics of Fiber and Textile Reinforced Cement Composites*; CRC Press: Boca Raton, FL, USA, 2011.
3. Mechtcherine, V.; Slowik, V.; Kabele, P. (Eds.) *Strain-Hardening Cement-Based Composites, SHCC4*; Springer: Berlin/Heidelberg, Germany, 2017; Volume 15.
4. Peled, A.; Bentur, A.; Mobasher, B. *Textile Reinforced Concrete*; CRC Press: Boca Raton, FL, USA, 2017; Volume 19.
5. Tomoscheit, S.; Gries, T.; Horstmann, M.; Hegger, J. Project life INSUSHELL: Reducing the carbon footprint in concrete construction. *Int. J. Sustain. Build. Technol. Urban Dev.* **2011**, *2*, 162–169. [[CrossRef](#)]
6. Williams Portal, N.; Lundgren, K.; Wallbaum, H.; Malaga, K. Sustainable potential of textile-reinforced concrete. *J. Mater. Civ. Eng.* **2015**, *27*, 04014207. [[CrossRef](#)]
7. Peled, A.; Mobasher, B. Pultruded fabric-cement composites. *ACI Mater. J.* **2005**, *102*, 15–23.
8. Peled, A.; Mobasher, B.; Cohen, Z. Mechanical properties of hybrid fabrics in pultruded cement composites. *Cem. Concr. Compos.* **2009**, *31*, 647–657. [[CrossRef](#)]
9. Häußler-Combe, U.; Jesse, F.; Curbach, M. Textile reinforced concrete-overview, experimental and theoretical investigations. In *Fracture Mechanics of Concrete Structures, Proceedings of the Fifth International Conference on Fracture Mechanics of Concrete and Concrete Structures, Ia-FraMCoS, Vail, CO, USA, 12–16 April 2004*; AEDIFICATIO Publications: Freiburg, Germany, 2004; Volume 204, pp. 12–16.
10. Jesse, F.; Will, N.; Curbach, M.; Hegger, J. Load-bearing behavior of textile-reinforced concrete. *Spec. Publ.* **2008**, *250*, 59–68.
11. Colombo, I.G.; Magri, A.; Zani, G.; Colombo, M.; Di Prisco, M. Erratum to: Textile Reinforced Concrete: Experimental investigation on design parameters. *Mater. Struct.* **2013**, *46*, 1953–1971. [[CrossRef](#)]
12. Rambo, D.A.S.; de Andrade Silva, F.; Toledo Filho, R.D.; Gomes, O.D.F.M. Effect of elevated temperatures on the mechanical behavior of basalt textile reinforced refractory concrete. *Mater. Des. (1980–2015)* **2015**, *65*, 24–33. [[CrossRef](#)]

13. Peled, A.; Bentur, A. Fabric structure and its reinforcing efficiency in textile reinforced cement composites. *Compos. Part A Appl. Sci. Manuf.* **2003**, *34*, 107–118. [[CrossRef](#)]
14. D'Antino, T.; Papanicolaou, C. Mechanical characterization of textile reinforced inorganic-matrix composites. *Compos. Part B Eng.* **2017**, *127*, 78–91. [[CrossRef](#)]
15. Hartig, J.; Häußler-Combe, U.; Schick Tanz, K. Influence of bond properties on the tensile behaviour of textile reinforced concrete. *Cem. Concr. Compos.* **2018**, *30*, 898–906. [[CrossRef](#)]
16. Häußler-Combe, U.; Hartig, J. Bond and failure mechanisms of textile reinforced concrete (TRC) under uniaxial tensile loading. *Cem. Concr. Compos.* **2007**, *29*, 279–289. [[CrossRef](#)]
17. Arboleda, D.; Carozzi, F.G.; Nanni, A.; Poggi, C. Testing procedures for the uniaxial tensile characterization of fabric reinforced cementitious matrix (FRCM) composites. *J. Compos. Constr.* **2016**, *20*, 04015063. [[CrossRef](#)]
18. Peled, A.; Zaguri, E.; Marom, G. Bonding characteristics of multifilament polymer yarns and cement matrices. *Compos. Part A Appl. Sci. Manuf.* **2008**, *39*, 930–939. [[CrossRef](#)]
19. Messori, M.; Nobili, A.; Signorini, C.; Sola, A. Mechanical performance of epoxy coated AR-glass fabric Textile Reinforced Mortar: Influence of coating thickness and formulation. *Compos. Part B Eng.* **2018**, *149*, 135–143. [[CrossRef](#)]
20. Bentur, A.; Tirosh, R.; Yardimci, M.; Puterman, M.; Peled, A. Controlling bond characteristics by impregnation. In Proceedings of the International RILEM Conference on Material Science, Aachen, Germany, 6–9 September 2010; RILEM Publications SARL: Paris, France, 2010; pp. 23–33.
21. Valeri, P.; Ruiz, M.F.; Muttoni, A. Tensile response of textile reinforced concrete. *Constr. Build. Mater.* **2020**, *258*, 119517. [[CrossRef](#)]
22. Donnini, J.; Corinaldesi, V.; Nanni, A. Mechanical properties of FRCM using carbon fabrics with different coating treatments. *Compos. Part B Eng.* **2016**, *88*, 220–228. [[CrossRef](#)]
23. Hegger, J.; Will, N.; Bruckermann, O.; Voss, S. Load-bearing behaviour and simulation of textile reinforced concrete. *Mater. Struct.* **2006**, *39*, 765–776. [[CrossRef](#)]
24. Raupach, M.; Orlowsky, J.; Büttner, T.; Dilthey, U.; Schleser, M.; Hegger, J. Epoxy-impregnated textiles in concrete-load bearing capacity and durability. In Proceedings of the 1st International RILEM Conference, Aachen, Germany, 6 September 2006; RILEM Publications SARL: Paris, France, 2006; pp. 77–88.
25. Paul, S.; Gettu, R.; Arnepalli, D.N.; Samanthula, R. Experimental evaluation of the durability of glass Textile-Reinforced Concrete. *Constr. Build. Mater.* **2023**, *406*, 133390. [[CrossRef](#)]
26. Butler, M.; Mechtcherine, V.; Hempel, S. Experimental investigations on the durability of fibre-matrix interfaces in textile-reinforced concrete. *Cem. Concr. Compos.* **2009**, *31*, 221–231. [[CrossRef](#)]
27. Kong, K.; Mesticou, Z.; Michel, M.; Larbi, A.S.; Junes, A. Comparative characterization of the durability behaviour of textile-reinforced concrete (TRC) under tension and bending. *Compos. Struct.* **2017**, *179*, 107–123. [[CrossRef](#)]
28. Caggegi, C.; Carozzi, F.G.; De Santis, S.; Fabbrocino, F.; Focacci, F.; Hojdys, Ł.; Lanoye, E.; Zuccarino, L. Experimental analysis on tensile and bond properties of PBO and aramid fabric reinforced cementitious matrix for strengthening masonry structures. *Compos. Part B Eng.* **2017**, *127*, 175–195. [[CrossRef](#)]
29. Mobasher, B.; Peled, A.; Pahilajani, J. Distributed cracking and stiffness degradation in fabric-cement composites. *Mater. Struct.* **2006**, *39*, 317–331. [[CrossRef](#)]
30. Bentur, A.; Yardimci, M.Y.; Tirosh, R. Preservation of telescopic bonding upon aging of bundled glass filaments by treatments with nano-particles. *Cem. Concr. Res.* **2013**, *47*, 69–77. [[CrossRef](#)]
31. Barhum, R.; Mechtcherine, V. Effect of short fibers on fracture behaviour of textile reinforced concrete. *Carbon* **2010**, *7*, 3950.
32. Barhum, R.; Mechtcherine, V. Influence of short dispersed and short integral glass fibers on the mechanical behaviour of textile-reinforced concrete. *Mater. Struct.* **2013**, *46*, 557–572. [[CrossRef](#)]
33. RILEM Technical Committee 232-TDT (Chair: W. Brameshuber). Recommendation of RILEM TC 232-TDT: Test methods and design of textile reinforced concrete: Uniaxial tensile test: Test method to determine the load bearing behavior of tensile specimens made of textile reinforced concrete. *Mater. Struct.* **2016**, *49*, 4923–4927. [[CrossRef](#)]
34. Hegger, J.; Voss, S. Investigations on the bearing behaviour and application potential of textile reinforced concrete. *Eng. Struct.* **2008**, *30*, 2050–2056. [[CrossRef](#)]
35. De Santis, S.; Carozzi, F.G.; de Felice, G.; Poggi, C. Test methods for Textile Reinforced Mortar systems. *Compos. Part B Eng.* **2017**, *127*, 121–132. [[CrossRef](#)]
36. Hartig, J.; Jesse, F.; Schick Tanz, K.; Häußler-Combe, U. Influence of experimental setups on the apparent uniaxial tensile load-bearing capacity of Textile Reinforced Concrete specimens. *Mater. Struct.* **2012**, *45*, 433–446. [[CrossRef](#)]
37. Leone, M.; Aiello, M.A.; Balsamo, A.; Carozzi, F.G.; Ceroni, F.; Corradi, M.; Gams, M.; Garbin, E.; Gattesco, N.; Krajewski, P.; et al. Glass fabric reinforced cementitious matrix: Tensile properties and bond performance on masonry substrate. *Compos. Part B Eng.* **2017**, *127*, 196–214. [[CrossRef](#)]
38. Contamine, R.; Larbi, A.S.; Hamelin, P. Contribution to direct tensile testing of textile reinforced concrete (TRC) composites. *Mater. Sci. Eng. A* **2011**, *528*, 8589–8598. [[CrossRef](#)]
39. Aveston, J.; Kelly, A. Theory of multiple fracture of fibrous composites. *J. Mater. Sci.* **1973**, *8*, 352–362. [[CrossRef](#)]
40. Cuypers, H.; Wastiels, J. A stochastic cracking theory for the introduction of matrix multiple cracking in textile reinforced concrete under tensile loading. In *Findings and Results from the Swedish Cyprus Expedition: A Gender Perspective at the Medelhavsmuseet*; RILEM: Stockholm, Sweden, 2006; pp. 193–202.

41. Li, B.; Xiong, H.; Jiang, J.; Dou, X. Tensile behavior of basalt textile grid reinforced Engineering Cementitious Composite. *Compos. Part B Eng.* **2019**, *156*, 185–200. [[CrossRef](#)]
42. Deng, M.; Dong, Z.; Zhang, C. Experimental investigation on tensile behavior of carbon textile reinforced mortar (TRM) added with short polyvinyl alcohol (PVA) fibers. *Constr. Build. Mater.* **2020**, *235*, 117801. [[CrossRef](#)]
43. Saidi, M.; Gabor, A. Iterative analytical modelling of the global behaviour of textile-reinforced cementitious matrix composites subjected to tensile loading. *Constr. Build. Mater.* **2020**, *263*, 120130. [[CrossRef](#)]
44. *ASTM D6637*; Standard Test Method for Determining Tensile Properties of Geogrids by the Single or Multi-Rib Tensile Method. American Society for Testing and Materials: West Conshohocken, PA, USA, 2015.
45. Soranakom, C.; Mobasher, B. Correlation of tensile and flexural responses of strain softening and strain hardening cement composites. *Cem. Concr. Compos.* **2008**, *30*, 465–477. [[CrossRef](#)]
46. Mobasher, B.; Dey, V.; Cohen, Z.; Peled, A. Correlation of constitutive response of hybrid textile reinforced concrete from tensile and flexural tests. *Cem. Concr. Compos.* **2014**, *53*, 148–161. [[CrossRef](#)]

Disclaimer/Publisher’s Note: The statements, opinions and data contained in all publications are solely those of the individual author(s) and contributor(s) and not of MDPI and/or the editor(s). MDPI and/or the editor(s) disclaim responsibility for any injury to people or property resulting from any ideas, methods, instructions or products referred to in the content.